Green's operator for a periodic medium with traction-free boundary conditions and computation of the effective properties of thin plates

T. K. Nguyen, Karam Sab, Guy Bonnet

▶ **To cite this version:**

T. K. Nguyen, Karam Sab, Guy Bonnet. Green's operator for a periodic medium with traction-free boundary conditions and computation of the effective properties of thin plates. International Journal of Solids and Structures, 2008, 45 (25-26), pp.6518-6534. hal-00691058

HAL Id: hal-00691058
https://hal.science/hal-00691058

Submitted on 28 Jan 2016

HAL is a multi-disciplinary open access archive for the deposit and dissemination of scientific research documents, whether they are published or not. The documents may come from teaching and research institutions in France or abroad, or from public or private research centers.

L'archive ouverte pluridisciplinaire **HAL**, est destinée au dépôt et à la diffusion de documents scientifiques de niveau recherche, publiés ou non, émanant des établissements d'enseignement et de recherche français ou étrangers, des laboratoires publics ou privés.

Green's operator for a periodic medium with traction-free boundary conditions and computation of the effective properties of thin plates

Trung-Kien Nguyen [a], Karam Sab [a,*], Guy Bonnet [b]

[a] Université Paris-Est, Institut Navier, LAMI, Ecole des Ponts, 6-8 Avenue Blaise Pascal, 77455 Marne-La-Vallée, France
[b] Université Paris-Est, Laboratoire de Modélisation et Simulation Multi Echelle (FRE3160 CNRS), Institut Navier, 5 bd Descartes, 77454 Marne-La-Vallée, France

A B S T R A C T

This paper presents a new Green's operator ($\boldsymbol{\Gamma}$-operator) for mixed periodic and stress-free boundary conditions. The solution is split into a classical periodic solution and a complementary solution to account for stress-free boundary conditions. This operator is used to obtain the effective properties of thin heterogeneous plates made of periodic cells, using the Fast Fourier Transform, the periodic thin plate theory and the computation of the strain energy within the cell. Numerical applications are provided, including comparisons with closed-form solutions and finite element solutions.

Keywords:
$\boldsymbol{\Gamma}$-operator
Green's function
Periodic thin plate homogenization
Fast Fourier Transform

1. Introduction

1.1. Effective properties and $\boldsymbol{\Gamma}$-operators

Theoretical and numerical methods which aim at obtaining the effective elastic properties of multiphase composite materials have been the subject of numerous studies. If one considers the case of periodic media, it is possible to show that the effective properties of heterogeneous materials can be obtained if the solution of an elasticity problem (localization problem) on the volume of a period subjected to periodicity boundary conditions and to "body forces" is solved. These body forces are computed from the heterogeneous elastic properties and from given macroscopic strains (see Sanchez-Palencia, 1974; Bakhvalov, 1974; Bensoussan et al., 1978; Auriault and Bonnet, 1985; Bakhvalov and Panasenko, 1989, and further references therein).

Similarly, if a representative elementary volume (REV) is considered, the effective properties can be obtained if the solution of an elasticity problem on the REV subjected to homogeneous boundary conditions (displacement null on the boundary for example) and to body forces is solved (see e.g. Kröner, 1971; Milton, 2002).

In both cases, it is possible to replace the problem on a volume containing heterogeneities by a sequence of problems characterized by body forces applied to a "homogeneous reference medium" and by homogeneous (or periodic) boundary conditions similar to those previously defined.

From another point of view, it is well known that the displacement which is solution of an elasticity problem characterized by homogeneous (or periodic) boundary conditions and by body forces can be expressed by using a Green's function. From the Green's function, an operator can be derived, allowing the computation of the strain field induced by a polarization tensor, the so-called $\boldsymbol{\Gamma}$-operator (see e.g. Milton, 2002) from the notation of the first authors using this operator (see e.g.

* Corresponding author. Tel.: +33 1 64 15 37 36; fax: +33 1 64 15 37 41.
E-mail address: sab@lami.enpc.fr (K. Sab).

Kröner, 1971; Willis, 1977), which is also named Green's operator by (Suquet, 1990; Moulinec and Suquet, 1994; Moulinec and Suquet, 1998). In the following, the name Γ-operator will be used. There is a close relation between the search of effective properties and the use of Γ-operators.]

Up to now such a strategy was restricted to the use of known Γ-operators: Γ-operator for an infinite domain and Γ-operator for periodic boundary conditions in the case of solutions related to a periodic cell. The main reason of such a situation is that Γ-operators for specific boundary conditions are known only for some special situations: infinite and semi-infinite domains, periodicity conditions, mixed boundary conditions... (see e.g. Seremet, 1991; Mura, 1991). In some cases, other specific boundary conditions must be considered: for example in the case of beams or plates, traction-free boundary conditions must be taken into account. In this case new Γ-operators are needed.

In a first step, this paper presents therefore the method for obtaining the Γ-operator which is well adapted to study a plate made of periodic cells: periodicity conditions along four faces and traction-free conditions along 2 faces for 3D problems, or periodicity conditions along two sides and traction-free conditions along two sides for 2D problems. This operator can obviously be used for other applications, for example to study the field generated by defects in elastic solids with given boundary conditions. This result has been therefore considered as the leading point of the paper.

1.2. Homogenization methods for periodic media

The second part of the paper is devoted to the use of the Γ-operator found in part 1 to develop new solutions for obtaining effective properties of plates made of periodically positioned cells. As explained previously, a rigorous procedure can be described in order to obtain the effective properties if a localization problem is solved on a period. Finite Element Method (FEM) has been used for the analysis of periodic materials. Most of the analyses are limited to simple microstructures. Recently, several authors studied more complex microstructures with inclusions of varying numbers and shapes (see Brockenbrough et al., 1991; Böhm et al., 1993; Gusev, 1997; Sab and Nedjar, 2005). The method needs however finite element meshings which are obviously tedious to implement, especially as soon as 3D computations are in view. To overcome this problem, several authors (Iwakuma and Nemat-Nasser, 1983; Luciano and Barbero, 1994; Cohen and Bergman, 2003) applied the method of Fourier series for calculating the effective properties of composites with a periodic microstructure. Kaßbohm et al. (2005), Kaßbohm et al. (2006) proposed an approximate method of Fourier coefficients for computing the properties of periodic structures with an arbitrary stiffness distribution. By using the Fast Fourier Transform (FFT), Suquet (1990), Moulinec and Suquet (1994), Moulinec and Suquet (1998), Michel et al. (1999) proposed an iterative numerical method to investigate the effective properties of linear and non-linear composites. The method was afterwards extended by Eyre and Milton (1999), by Michel et al. (2001) and by Moulinec and Suquet (2003). This method makes direct use of digital images of the microstructure of the composites. It is based on the exact expression of the Γ-operator for a linear isotropic elastic homogeneous material and periodic boundary conditions. A part of the efficiency of this method is due to the use of FFT packages, which allows to reduce the calculation times and to analyze the plane (2D) or volumic (3D) periodic complex microstructures without FEM meshing. Using discrete Fourier transforms, Neumann et al. (2001), Neumann et al. (2002) presented also a method for the analysis of heterogeneous bodies. Bonnet (2007) proposed an explicit series solution for the calculation of the effective properties of composites having periodically positioned heterogeneities by using Neuman series and exact expressions of the shape factors in Fourier space. Recent studies using the Fourier method and FFT algorithms showed their efficiency when used for obtaining the effective properties of periodic media.

The homogenization of elastic periodic plates has been studied by many authors (Duvaut and Metellus, 1976; Caillerie, 1984; Kohn and Vogelius, 1984; Lewiński and Telega,1999; Cecchi and Sab, 2002a,b, 2004). Two characteristic length scales coexist: the typical size L of the plate and its thickness t. Moreover, the in-plane periodicity of the structure introduces an additional characteristic length ϵ which describes the in-plane size of the unit cell that generates the plate by periodicity. For a fixed value of L, the homogenization problem consists in finding the asymptotic solution when t and ϵ tend to zero. As shown in Caillerie (1984) and Kohn and Vogelius (1984), the homogenization scheme depends on the relative rate of convergence towards zero of t and ϵ. It is generally assumed that ϵ is a function of t which behaves likes t^a with $a > 0$ when t is small. Three cases have been considered: $a < 1, a = 1$ and $a > 1$. If $a < 1$, the 3D heterogeneous structure is replaced by a periodic Love–Kirchhoff plate whose elastic properties are periodic ($t \to 0$). The properties of the equivalent homogeneous plate are then obtained by a homogenization process applied to plate properties ($\epsilon \to 0$). First results on the homogenization of Love–Kirchhoff plates are due to Duvaut and Metellus (1976). If $a > 1$, the properties of the 3D heterogeneous structure are obtained in a first step by a homogenization process ($\epsilon \to 0$) and the resulting homogeneous 3D-body is then replaced by a 2D plate ($t \to 0$). Finally, in the case $a = 1$ (the in-plane size of the unit cell is comparable to the thickness of the plate: $t \sim \epsilon \to 0$), the 3D heterogeneous body is replaced by a homogeneous Love–Kirchhoff plate whose stiffness constants are computed by solving an auxiliary boundary problem on the 3D unit cell. This approach has been extended to the limit analysis of periodic plates by Bourgeois et al. (1998), Sab (2003), Dallot and Sab (2008a), Dallot and Sab (2008b).

The objective of this paper is to present a new approach for obtaining the effective elastic properties of periodic thin plates. The thickness and the period of the plate are assumed to be of the same order and much smaller than the in-plane typical characteristic size L of the plate (case $a = 1$). The stiffness constants of the plate can thus be computed by solving a boundary value problem on a unit cell. The Fast Fourier Transform method is used to solve the problem. The solution is split into a classical periodic solution and a complementary solution to account for the traction-free boundary conditions. The effective elastic properties of the plate are finally obtained by the calculation of strain energy in which the strain and stress

fields are obtained by a basic iterative algorithm. The numerical validation of the method is then performed in the case of two numerical examples.

2. Related Γ-operators

This section aims at formulating a new Γ-operator for periodic media with traction-free boundary conditions. To do so, the first two subsections will summarize known operators and can be considered as a review of known results: for an infinite medium (Kröner, 1971; Willis, 1977, 1980, 1981) and for a periodic medium (Suquet, 1990; Moulinec and Suquet, 1994, 1998).

2.1. Γ-operator for an infinite medium

Let us consider a homogeneous infinite elastic medium characterized by the stiffness $\mathbf{L}^o$ and subjected to a pre-stress field $\boldsymbol{\tau}(\mathbf{x})$.

The equilibrium equation can be written as:

$$\boldsymbol{\sigma}(\mathbf{x}) \cdot \boldsymbol{\nabla} = 0, \tag{1}$$

where the stress field may be split into an elastic part and a pre-stress part $\boldsymbol{\tau}(\mathbf{x})$ as:

$$\boldsymbol{\sigma}(\mathbf{x}) = \mathbf{L}^o : \mathbf{e}(\mathbf{x}) + \boldsymbol{\tau}(\mathbf{x}), \tag{2}$$

where the strain field $\mathbf{e}(\mathbf{x})$ is linearly related to the displacement field $\mathbf{u}(\mathbf{x})$ by:

$$\mathbf{e}(\mathbf{x}) = \mathbf{u}(\mathbf{x}) \otimes^s \boldsymbol{\nabla}, \tag{3}$$

where the nabla operator $\boldsymbol{\nabla}$ is used to express the gradient and divergence operators ($\mathbf{u} \otimes \boldsymbol{\nabla} = u_{i,j}\, \mathbf{e}_i \otimes \mathbf{e}_j$, $\boldsymbol{\sigma} \cdot \boldsymbol{\nabla} = \sigma_{ij,j}\, \mathbf{e}_i$). The Greek indices are assumed to range within $\{1,2\}$ while the Latin indices take values $\{1,2,3\}$. The $\mathbf{e}_i$ are the vectors of an orthogonal basis of the space, $\mathbf{u}(\mathbf{x})$ is the displacement field, $\mathbf{e}(\mathbf{x})$ the corresponding strain field (the symmetrical part $\mathbf{u}(\mathbf{x}) \otimes^s \boldsymbol{\nabla}$ of $\mathbf{u}(\mathbf{x}) \otimes \boldsymbol{\nabla}$), $\boldsymbol{\sigma}(\mathbf{x})$ the total stress field.

$\mathbf{L}^o$ is a uniform elasticity tensor given, in the case of an isotropic medium, by:

$$\mathbf{L}^o : \mathbf{e}(\mathbf{x}) = \lambda \operatorname{tr}(\mathbf{e}(\mathbf{x}))\, \mathbf{1} + 2\mu \mathbf{e}(\mathbf{x}).$$

The prestressed field or "polarization field" $\tau(\mathbf{x})$, may come from an eigenstrain due to thermal expansion, plasticity or other physical phenomena (see e.g. Mura, 1991; Bornert et al., 2001).

Substituting (2) into (1) leads to:

$$(\mathbf{L}^o : \mathbf{e}(\mathbf{x})) \cdot \boldsymbol{\nabla} + \boldsymbol{\tau}(\mathbf{x}) \cdot \boldsymbol{\nabla} = 0. \tag{4}$$

For a given polarization stress field $\boldsymbol{\tau}(\mathbf{x})$, the solution of Eq. (4) in an infinite medium can be expressed by using a non-local Γ-operator of the linear homogeneous medium $\mathbf{L}^o$ as:

$$\mathbf{e}(\mathbf{x}) = -\int \boldsymbol{\Gamma}(\mathbf{x} - \mathbf{x}')\, \boldsymbol{\tau}(\mathbf{x}')\, \mathrm{d}\mathbf{x}', \tag{5}$$

where the Γ-operator is related to the Green's function of the infinite homogeneous body $\mathbf{G}$ (Kelvin's tensor for an isotropic medium for example) by:

$$\Gamma_{ijkl}(\mathbf{x} - \mathbf{x}') = -\mathbf{G}_{jk,il}(\mathbf{x} - \mathbf{x}'), \tag{6}$$

and it is noted that the fourth-order tensor possesses the symmetry on the indices (ij), (kl).

The Green's function of the infinite homogeneous $\mathbf{G}(\mathbf{x})$ is itself the solution of the following differential equation:

$$L^o_{ijkl} G_{mk,lj}(\mathbf{x}) + \delta_{mi}\, \delta(\mathbf{x}) = 0. \tag{7}$$

It is well known that the Green's function $\mathbf{G}(\mathbf{x})$ is characterized by a $1/r$ singularity for 3D and a logarithmic singularity $\ln(r)$ for the 2D case, where $r = |\, \mathbf{x} - \mathbf{x}'\, |$. The Γ-operator is therefore strongly singular. The convolution product in (5) is very difficult to estimate in the real space and it is therefore in many cases more suitable to use the Fourier transforms of $\mathbf{G}$ and $\boldsymbol{\Gamma}$.

The Γ-operator and the corresponding strain defined in (6) and (5) will be therefore obtained by using Fourier transforms. The Fourier transform of $f(\mathbf{x})$ and its inverse are defined as:

$$\hat{f}(\mathbf{k}) = \int f(\mathbf{x})\, \mathrm{e}^{-\mathrm{i}\mathbf{k}\cdot\mathbf{x}}\, \mathrm{d}\mathbf{x}, \quad f(\mathbf{x}) = \frac{1}{8\pi^3} \int \hat{f}(\mathbf{k})\, \mathrm{e}^{\mathrm{i}\mathbf{k}\cdot\mathbf{x}}\, \mathrm{d}\mathbf{k}, \tag{8}$$

where all the integrals are taken on $\mathbf{R}^3$. The index i denotes the complex number ($\mathrm{i} = \sqrt{-1}$). $\mathbf{k} = (k_1, k_2, k_3)$ is the wave-vector. $\mathbf{k} \cdot \mathbf{x}$ is a scalar product. The 3-dimensional Fourier transforms of (6) and (7) lead to:

$$\widehat{\Gamma}_{ijkl}(\mathbf{k}) = k_i k_l \widehat{G}_{jk}(\mathbf{k}) \quad \text{and} \quad -L^o_{ijkl}\, \widehat{G}_{mk}(\mathbf{k}) k_l k_j + \delta_{mi} = 0. \tag{9}$$

By setting $K^o_{ik}(\mathbf{k}) = L^o_{ijkl}k_l k_j$ which are components of the acoustic tensor of the homogeneous material and by naming $N^o(\mathbf{k})$ the inverse of $K^o(\mathbf{k})$, the operator $\boldsymbol{\Gamma}$ can be expressed in the Fourier domain as:

$$\widehat{\Gamma}_{ijkl}(\mathbf{k}) = \frac{1}{4}(N^o_{ik}(\mathbf{k})k_j k_l + N^o_{il}(\mathbf{k})k_j k_k + N^o_{jk}(\mathbf{k})k_i k_l + N^o_{jl}(\mathbf{k})k_i k_k). \tag{10}$$

The Fourier components of the $\boldsymbol{\Gamma}$-operator are explicitly given for different types of anisotropy of the homogeneous medium (see e.g. Willis, 1977, 1980, 1981; Mura, 1991). For an isotropic material with Lamé coefficients (λ, μ), it takes the form:

$$\widehat{\Gamma}_{ijkl} = \frac{1}{4\mu|\mathbf{k}|^2}(\delta_{ik}k_j k_l + \delta_{jk}k_i k_l + \delta_{il}k_j k_k + \delta_{jl}k_i k_k) - \frac{\lambda+\mu}{\mu(\lambda+2\mu)}\frac{k_i k_j k_k k_l}{|\mathbf{k}|^4}. \tag{11}$$

2.2. Case of periodic boundary conditions

Let us now consider a periodic medium characterized by a basic cell Y. Any periodic function $f(\mathbf{x})$ can be expanded into the Fourier series:

$$f(\mathbf{x}) = \sum_{\mathbf{k}} \hat{f}(\mathbf{k})\, e^{i\mathbf{k}\cdot\mathbf{x}}, \quad \hat{f}(\mathbf{k}) = \frac{1}{|Y|}\int_Y f(\mathbf{x})\, e^{-i\mathbf{k}\cdot\mathbf{x}}\, d\mathbf{x}, \tag{12}$$

where the tips of discrete wave-vectors $\mathbf{k}$ are points of the reciprocal lattice.

If one considers now a periodic polarization tensor $\boldsymbol{\tau}$, it is possible to define the periodic $\boldsymbol{\Gamma}$-operator and the corresponding strains along the same lines as those used for the infinite medium. After Fourier transform of Eqs. ()(1)–(3) and elimination of $\hat{\sigma}_{ij}$ between the equations, the expression of operator $\boldsymbol{\Gamma}$ has finally the same form as (10). The periodic strain field of the problem can then be obtained in the real space $\mathbf{e}^p(\mathbf{x})$ and the Fourier space $\hat{\mathbf{e}}^p(\mathbf{k})$ by means of the periodic $\boldsymbol{\Gamma}$-operator associated with the homogeneous elastic medium with stiffness $\mathbf{L}^o$ (see Suquet, 1990; Moulinec and Suquet, 1994, 1998),

$$\begin{aligned} &\text{In real space :} \qquad \mathbf{e}^p(\mathbf{x}) = -\boldsymbol{\Gamma} * \boldsymbol{\tau}(\mathbf{x}). \\ &\text{In Fourier space :} \quad \hat{\mathbf{e}}^p(\mathbf{k}) = -\widehat{\boldsymbol{\Gamma}}(\mathbf{k}) : \hat{\boldsymbol{\tau}}(\mathbf{k}) \quad \forall \mathbf{k}\neq 0,\ \hat{\mathbf{e}}^p(0) = 0. \end{aligned} \tag{13}$$

In this case the strain field given by (13) complies obviously to boundary conditions along the periodic boundaries of Y.

2.3. Periodic boundary conditions mixed with traction-free boundary conditions

Let us now consider a basic cell Y. Mixed conditions are defined along the boundaries of the cell as follows: periodic boundary conditions are assumed along the boundaries perpendicular to x_1 and x_2 while traction-free boundary conditions are assumed along the boundary perpendicular to x_3. The domain Y of the cell is defined by:

$$Y = \left\{ \mathbf{x} \in \mathbf{R}^3,\ \mathbf{x} = (x_1, x_2, x_3), \quad x_1 \in]0, l_1[, \quad x_2 \in]0, l_2[, \quad x_3 \in \left]-\frac{t}{2}, \frac{t}{2}\right[\right\}. \tag{14}$$

The domain $\omega =]0, l_1[\times]0, l_2[$ is the middle surface of the cell with the boundary $\partial\omega$ and $\partial Y_l = \partial\omega \times \left]-\frac{t}{2}, \frac{t}{2}\right[$ is the lateral boundary of Y. The top and bottom surfaces of the cell are denoted by $\partial Y^{\pm} = \omega \times \{\pm\frac{t}{2}\}$. All formulations are performed under the assumption of a linear elastic behavior and small deformations of materials.

For a given periodic polarization $\boldsymbol{\tau}$, the problem which must be solved on Y is now defined in the following form:

$$\begin{cases} \boldsymbol{\sigma}(\mathbf{x}) \cdot \nabla = 0, \quad \boldsymbol{\sigma}(\mathbf{x}) = \mathbf{L}^o : \mathbf{e}(\mathbf{x}) + \boldsymbol{\tau}(\mathbf{x}), \\ \mathbf{e}(\mathbf{x}) = \mathbf{u}(\mathbf{x}) \otimes^s \nabla, \\ \mathbf{u}(\mathbf{x}) \text{ periodic on } \partial Y_l, \quad \boldsymbol{\sigma}(\mathbf{x}) \cdot \mathbf{n} \text{ antiperiodic on } \partial Y_l, \end{cases} \tag{15}$$

and traction-free boundary conditions on $\partial Y^{\pm}$ are assumed,

$$\boldsymbol{\sigma} \cdot \mathbf{e}_3 = 0 \quad \text{on} \quad \partial Y^{\pm}. \tag{16}$$

For $\tau(\mathbf{x}) \in \mathbf{L}^2(Y)$, the boundary value problem (15 and 16) can be solved by expanding the polarization stress into the Fourier series defined in (12),

$$\boldsymbol{\tau}(\mathbf{x}) = \sum_{\mathbf{k}} \hat{\boldsymbol{\tau}}(\mathbf{k})\, e^{i\mathbf{k}\cdot\mathbf{x}}, \tag{17}$$

where the coefficients of the Fourier series $\hat{\tau}(\mathbf{k})$ can be calculated by the Fast Fourier Transform (FFT) (see e.g. Soize, 1993; Gasquet and Witomski, 2000; Kaßbohm et al., 2005).

The solution $\mathbf{u}(\mathbf{x})$ of the problem (15 and 16) can be split into two terms: the first term can be obtained with the standard periodicity conditions in the direction x_3 (as in the previous section) and the second term is the complement which is necessary to comply to the traction-free boundary conditions:

$$\mathbf{u}(\mathbf{x}) = \mathbf{u}^p(\mathbf{x}) + \mathbf{u}^h(\mathbf{x}),$$

with,

$$\mathbf{u}^p(\mathbf{x}) = \sum_{\mathbf{k}} \hat{\mathbf{u}}^p(\mathbf{k})\, \mathrm{e}^{\mathrm{i}\mathbf{k}\cdot\mathbf{x}}, \quad \mathbf{u}^h(\mathbf{x}) = \sum_{\tilde{\mathbf{k}}} \tilde{\mathbf{u}}^h(\tilde{\mathbf{k}}, x_3)\, \mathrm{e}^{\mathrm{i}k_\alpha x_\alpha}, \tag{18}$$

where $\tilde{\mathbf{k}} = (k_1, k_2)$, $\mathbf{k} = (k_1, k_2, k_3)$ are the discrete wave vectors arranged along a discrete lattice having a period $2\pi/l_i$ ($l_3 = t$) along the direction x_i.

$\mathbf{u}^p(\mathbf{x})$ is the solution of the problem (15) with full periodicity conditions for which the corresponding strain $\mathbf{e}^p(\mathbf{x})$ is defined in (13) and the stress field is then expressed in the Fourier space as follows:

$$\hat{\boldsymbol{\sigma}}^p(\mathbf{k}) = \lambda \mathrm{tr}(\hat{\mathbf{e}}^p(\mathbf{k}))\, \mathbf{1} + 2\mu \hat{\mathbf{e}}^p(\mathbf{k}) + \hat{\boldsymbol{\tau}}(\mathbf{k}).$$

The complementary displacement field $\mathbf{u}^h(\mathbf{x})$ which is necessary to comply to the traction-free boundary conditions is obtained by using the following system of equations:

$$\begin{cases} \boldsymbol{\sigma}^h(\mathbf{x}) \cdot \boldsymbol{\nabla} = 0, \quad \boldsymbol{\sigma}^h(\mathbf{x}) = \mathbf{L}^o : \mathbf{e}^h(\mathbf{x}), \\ \mathbf{e}^h(\mathbf{x}) = \mathbf{u}^h(\mathbf{x}) \otimes^s \boldsymbol{\nabla}, \\ \sigma^h_{j3}(x_1, x_2, x_3 = \pm\frac{t}{2}) = -\sigma^p_{j3}(x_1, x_2, x_3 = \pm\frac{t}{2}), \\ \mathbf{u}^h(\mathbf{x}) \text{ periodic on } \partial Y_l, \quad \boldsymbol{\sigma}^h(\mathbf{x}) \cdot \mathbf{n} \text{ antiperiodic on } \partial Y_l. \end{cases} \tag{19}$$

The solution of problem (19), complying to periodic boundary condition along the boundaries which are perpendicular to x_1 and x_2, may be expanded into the Fourier series as expressed in the second term of (18) where $\tilde{\mathbf{u}}^h(\tilde{\mathbf{k}}, x_3)$ has to be obtained. The corresponding strains and stresses are, respectively:

$$\mathbf{e}^h(\mathbf{x}) = \sum_{\tilde{\mathbf{k}}} \tilde{\mathbf{e}}^h(\tilde{\mathbf{k}}, x_3)\, \mathrm{e}^{\mathrm{i}k_\alpha x_\alpha}, \quad \boldsymbol{\sigma}^h(\mathbf{x}) = \sum_{\tilde{\mathbf{k}}} \tilde{\boldsymbol{\sigma}}^h(\tilde{\mathbf{k}}, x_3)\, \mathrm{e}^{\mathrm{i}k_\alpha x_\alpha}. \tag{20}$$

The strain field is related to the displacement field by:

$$\tilde{\mathbf{e}}^h(\tilde{\mathbf{k}}, x_3) = \tilde{\mathbf{u}}^h(\tilde{\mathbf{k}}, x_3) \otimes^s \boldsymbol{\nabla}', \tag{21}$$

where the operator $\boldsymbol{\nabla}'$ is defined by $\boldsymbol{\nabla}' = [\mathrm{i}k_1 \quad \mathrm{i}k_2 \quad \partial_3]^{\mathrm{T}}$. The operator ∂ indicates the partial differentiation with respect to the coordinate subscript that follows. The stress field is obtained from the constitutive equations:

$$\tilde{\boldsymbol{\sigma}}^h(\tilde{\mathbf{k}}, x_3) = \lambda(\tilde{\mathbf{u}}^h(\tilde{\mathbf{k}}, x_3).\boldsymbol{\nabla}')\, \mathbf{1} + 2\mu(\tilde{\mathbf{u}}^h(\tilde{\mathbf{k}}, x_3) \otimes^s \boldsymbol{\nabla}'). \tag{22}$$

The equilibrium equation $\boldsymbol{\sigma}^h(\mathbf{x}) \cdot \boldsymbol{\nabla} = 0$ becomes $\tilde{\boldsymbol{\sigma}}^h(\tilde{\mathbf{k}}, x_3) \cdot \boldsymbol{\nabla}' = 0$ which leads to:

$$[(\lambda + \mu)\boldsymbol{\nabla}' \otimes^s \boldsymbol{\nabla}' + \mu(\boldsymbol{\nabla}' \cdot \boldsymbol{\nabla}')\, \mathbf{1}].\, \tilde{\mathbf{u}}^h(\tilde{\mathbf{k}}, x_3) = 0, \tag{23}$$

where,

$$\boldsymbol{\nabla}' \otimes^s \boldsymbol{\nabla}' = \begin{bmatrix} -k_1^2 & -k_1 k_2 & \mathrm{i}k_1 \partial_3 \\ -k_1 k_2 & -k_2^2 & \mathrm{i}k_2 \partial_3 \\ \mathrm{i}k_1 \partial_3 & \mathrm{i}k_2 \partial_3 & \partial_{33}^2 \end{bmatrix}, \quad \boldsymbol{\nabla}' \cdot \boldsymbol{\nabla}' = \partial_{33}^2 - (k_1^2 + k_2^2). \tag{24}$$

The solution of Eq. (23) is (see Appendix A.1):

$$\tilde{\mathbf{u}}^h(\tilde{\mathbf{k}}, x_3) = (\mathbf{a}^+ + x_3 \mathbf{b}^+)\, \mathrm{e}^{sx_3} + (\mathbf{a}^- + x_3 \mathbf{b}^-)\, \mathrm{e}^{-sx_3}, \tag{25}$$

where:

$$\mathbf{a}^\pm = \begin{Bmatrix} a_1^\pm \\ a_2^\pm \\ \pm\frac{1}{\mathrm{i}s}(a_1^\pm k_1 + a_2^\pm k_2 - \mathrm{i}\frac{\lambda+3\mu}{\lambda+\mu} b_3^\pm) \end{Bmatrix}, \quad \mathbf{b}^\pm = \begin{Bmatrix} \pm\frac{\mathrm{i}k_1}{s} b_3^\pm \\ \pm\frac{\mathrm{i}k_2}{s} b_3^\pm \\ b_3^\pm \end{Bmatrix}, \quad s = \sqrt{k_1^2 + k_2^2}. \tag{26}$$

The six complex coefficients $(a_1^\pm, a_2^\pm, b_3^\pm)$ are obtained from the six boundary conditions defined in (19) which are rewritten as follows:

$$\tilde{\sigma}^h_{j3}\left(\tilde{\mathbf{k}}, \pm\frac{t}{2}\right) = -\sum_{k_3} \hat{\sigma}^p_{j3}(\mathbf{k}) \mathrm{e}^{\pm \mathrm{i}k_3 \frac{t}{2}}. \tag{27}$$

The previous relation leads to the explicit expressions of $(a_1^\pm, a_2^\pm, b_3^\pm)$ as follows:

$$\begin{aligned} b_3^\pm &= w^\pm g^+ + w^\mp g^-, \\ a_2^\pm &= -\frac{\mathrm{i}k_2}{2s^2 \sinh(st)}\left(c_1 b_3^\pm + stb_3^\mp\right) \pm \frac{s^2 + k_1^2}{4s^4 \sinh(st)}(q_2^\pm \mathrm{e}^{\frac{qt}{2}} - q_2^\mp \mathrm{e}^{-\frac{qt}{2}}) \mp \frac{k_1 k_2}{4s^4 \sinh(st)}(q_1^\pm \mathrm{e}^{\frac{qt}{2}} - q_1^\mp \mathrm{e}^{-\frac{qt}{2}}), \\ a_1^\pm &= -\frac{k_1 k_2}{s^2 + k_1^2} a_2^\pm - \frac{\mathrm{i}k_1}{(s^2 + k_1^2)\sinh(st)}\left(c_1 b_3^\pm + stb_3^\mp\right) \pm \frac{1}{2(s^2 + k_1^2)\sinh(st)}(q_1^\pm \mathrm{e}^{\frac{qt}{2}} - q_1^\mp \mathrm{e}^{-\frac{qt}{2}}), \end{aligned} \tag{28}$$

where:

$$
\begin{aligned}
q_1^{\pm} &= -\sum_{k_3} \frac{S}{\mu} e^{\pm ik_3 \frac{t}{2}} \hat{\sigma}_{13}^p(\mathbf{k}),\\
q_2^{\pm} &= -\sum_{k_3} \frac{S}{\mu} e^{\pm ik_3 \frac{t}{2}} \hat{\sigma}_{23}^p(\mathbf{k}),\\
q_3^{\pm} &= -\sum_{k_3} e^{\pm ik_3 \frac{t}{2}} \hat{\sigma}_{33}^p(\mathbf{k}),\\
w^{\pm} &= \mp \frac{e^{\pm \frac{st}{2}} \sinh(st) + ste^{\mp \frac{st}{2}}}{4\mu(\sinh^2(st) - s^2t^2)}, \quad c_1 = \left(\frac{st}{2} - \frac{\mu}{\lambda+\mu}\right) e^{st} + \left(\frac{st}{2} + \frac{\mu}{\lambda+\mu}\right) e^{-st},\\
g^{\pm} &= q_3^{\pm} \pm \frac{i\mu}{s^2 \sinh(st)} [(k_1 q_1^{\pm} + k_2 q_2^{\pm}) \cosh(st) - (k_1 q_1^{\mp} + k_2 q_2^{\mp})].
\end{aligned}
\tag{29}
$$

The derivation of the displacement field (Eqs. (25) and (26)) and the calculation of the coefficients $(a_1^{\pm}, a_2^{\pm}, b_3^{\pm})$ from the boundary condition (27) are given in Appendix A.1. The complementary strain field $\tilde{\mathbf{e}}^h(\tilde{\mathbf{k}}, x_3)$ is then obtained by (21).

The total strain field is a combination of the two components obtained from (13) and (21):

$$
\mathbf{e}(\mathbf{x}) = \mathbf{e}^p(\mathbf{x}) + \mathbf{e}^h(\mathbf{x}), \tag{30}
$$

where,

$$
\mathbf{e}^p(\mathbf{x}) = \sum_{\mathbf{k}} \tilde{\mathbf{e}}^p(\mathbf{k}) e^{i\mathbf{k}\cdot\mathbf{x}}, \quad \mathbf{e}^h(\mathbf{x}) = \sum_{\tilde{\mathbf{k}}} \tilde{\mathbf{e}}^h(\tilde{\mathbf{k}}, x_3) e^{ik_\alpha x_\alpha}. \tag{31}
$$

Expression (26) shows that the coefficients $(a_1^{\pm}, a_2^{\pm}, b_3^{\pm})$ and the complementary displacement field $\tilde{\mathbf{u}}^h(\tilde{\mathbf{k}}, x_3)$ must be obtained also for $s \neq 0$ or $|\tilde{\mathbf{k}}| \neq 0$. As a result, the corresponding strain field $\tilde{\mathbf{e}}^h(\tilde{\mathbf{k}}, x_3)$ is obtained. The complete expression of the strains $\tilde{\mathbf{e}}^h(\tilde{\mathbf{k}}, x_3)$ is given in Appendix A.2.

Finally, the strain field is related to the polarization field via a $\boldsymbol{\Gamma}$-operator which can be considered as a projection of the polarizations onto the strains. The previous formulations enable to construct a new $\boldsymbol{\Gamma}$-operator for the mixed boundary conditions. In fact, for a given polarization field, the total strain field is obtained from Eqs. (30) and (31) where the complementary strain field is calculated by expressions (21), (25) and (28), while the periodic strain field is defined classically by (13). This step will be used in the following part to obtain the effective elastic properties of a thin plate.

3. Application to thin plate homogenization

Let us consider a Love–Kirchhoff heterogeneous plate having a thickness t which is located within a domain $\Omega \times]-\frac{t}{2}, \frac{t}{2}[$, $t \in R^+$. $\Omega \in \mathbf{R}^2$ is the middle surface of the plate. The plate exhibits a periodic structure in directions x_1 and x_2 so that it is possible to extract an elementary cell Y given by (14) which contains all the information necessary to completely describe the plate and more precisely the value of the elasticity tensor $\mathbf{L}(\mathbf{x})$ at each point. It is assumed that the thickness of the plate and the typical length of the cell are of the same order, and that they are very small in comparison with the in-plane typical length of the plate.

The "homogenization problem" on Y is defined as follows:

$$
\begin{cases}
\boldsymbol{\sigma}(\mathbf{x}) \cdot \mathbf{V} = 0, \quad \boldsymbol{\sigma}(\mathbf{x}) = \mathbf{L}(\mathbf{x}) : \boldsymbol{\epsilon}(\mathbf{x}),\\
\boldsymbol{\epsilon}(\mathbf{x}) = \mathbf{E} + x_3 \boldsymbol{\chi} + \mathbf{e}(\mathbf{u}(\mathbf{x})),\\
\mathbf{u}(\mathbf{x}) \text{ periodic on } \partial Y_l, \quad \boldsymbol{\sigma}(\mathbf{x}) \cdot \mathbf{n} \text{ antiperiodic on } \partial Y_l,
\end{cases}
\tag{32}
$$

and the free boundary conditions on $\partial Y^{\pm}$ are assumed,

$$
\boldsymbol{\sigma} \cdot \mathbf{e}_3 = 0 \quad \text{on} \quad \partial Y^{\pm}. \tag{33}
$$

This problem allows to obtain the stiffness properties related to the macroscopic kinematics defined by the"in plane" membrane strain $\mathbf{E}$ and the curvature $\boldsymbol{\chi}$ of the middle surface of the plate. The problem (32 and 33) is transformed into the boundary value problem (15 and 16) defined in the previous section by introducing a homogeneous elastic reference medium $\mathbf{L}^o$, leading to the polarization field $\boldsymbol{\tau}(\mathbf{x})$ given by:

$$
\boldsymbol{\tau}(\mathbf{x}) = \mathbf{L}(\mathbf{x}) : [\mathbf{E} + x_3 \boldsymbol{\chi} + \mathbf{e}(\mathbf{u}(\mathbf{x}))] - \mathbf{L}^o : \mathbf{e}(\mathbf{u}(\mathbf{x})). \tag{34}
$$

The strain field $\mathbf{e}(\mathbf{u}(\mathbf{x}))$, symmetrical part of $\mathbf{u}(\mathbf{x}) \otimes \mathbf{V}$, will be denoted simply by $\mathbf{e}(\mathbf{x})$ in the following. The "macroscopic" fields $\mathbf{E}$ and $\boldsymbol{\chi}$ have only the in-plane components: $E_{j3} = 0$, $\chi_{j3} = 0$ (see Caillerie, 1984).

The boundary value problem (32)–(34) has the same structure as the basic problem (15 and 16). The polarization tensor is now a function of the unknown strain field. Eqs. (32) and (33) are therefore solved by using a basic iterative procedure. At each iteration, the polarization field is given by (34).

3.1. Homogenization procedure

The homogenized elastic properties of the plate are obtained from the elastic strain energy per unit area of the plate expressed by:

$$\frac{1}{2|\omega|}\int \boldsymbol{\sigma}(\mathbf{x}) : \boldsymbol{\epsilon}(\mathbf{x})\,\mathrm{d}Y = \frac{1}{2}(\mathbf{N}\mathbf{E} + \mathbf{M}\boldsymbol{\chi}). \tag{35}$$

$\mathbf{N}$ is the membrane stress tensor and $\mathbf{M}$ is the flexure moment tensor:

$$N_{\alpha\beta} = \frac{1}{|\omega|}\int \sigma_{\alpha\beta}\,\mathrm{d}Y, \quad M_{\alpha\beta} = \frac{1}{|\omega|}\int x_3\,\sigma_{\alpha\beta}\,\mathrm{d}Y. \tag{36}$$

Eq. (35) can be interpreted as the macro-homogeneity condition of Hill-Mandel which ensures that the macroscopic elastic strain energy of a given representative volume element is equal to the integral of the microscopic elastic strain energy within this volume.

Hence, the strain energy per unit area becomes:

$$\frac{1}{2|\omega|}\int \boldsymbol{\sigma}(\mathbf{x}) : \boldsymbol{\epsilon}(\mathbf{x})\,\mathrm{d}Y = \frac{1}{2}(\mathbf{E}\mathbf{A}\mathbf{E} + 2\mathbf{E}\mathbf{B}\boldsymbol{\chi} + \boldsymbol{\chi}\mathbf{D}\boldsymbol{\chi}). \tag{37}$$

It can be seen that the homogenized stiffness properties $(\mathbf{A}, \mathbf{B}, \mathbf{D})$ of the plate will be obtained by using an appropriate choice of the macroscopic tensors $(\mathbf{E}, \boldsymbol{\chi})$ and by calculating the elastic strain energy.

The discrete Fourier transform is performed by discretization of the cell Y into a regular grid: $(N_1 \times N_2)$ points (pixels – 2D problems) or $(N_1 \times N_2 \times N_3)$ points (voxels - 3D problems). For two-dimensional problems in the space (x_1, x_3), the coordinates in the real space are defined by:

$$x_1 = (i_1 - 1)\cdot\frac{l_1}{N_1}, \quad i_1 = 1, \ldots, N_1 \quad \text{and} \quad x_3 = i_3\cdot\frac{t}{N_3}, \quad i_3 = -\frac{N_3}{2}, \ldots, 0, \ldots, \frac{N_3}{2} - 1. \tag{38}$$

This discretization is appropriate for using the Fast Fourier Transform (FFT) as soon as N_i are powers of 2. The computation of the FFT corresponds to the wave-number orders $n_i = [0, \ldots, \frac{N_i}{2} - 1, -\frac{N_i}{2}, \ldots, -1]$. The components of the wave vectors are then defined as follows:

$$k_1 = \frac{2\pi n_1}{l_1}, \quad k_3 = \frac{2\pi n_3}{t}. \tag{39}$$

This discretization will be used for the analysis of the plane strain problems studied in the following section.

3.2. Iterative algorithm

The boundary value problem (32 and 33) is solved by using the method proposed in Section 2.3 with a given polarization field in (34). The iterative algorithm necessary to compute the strain and stress fields of the problem (32), (33) comprises the steps described below for the 3D case:

Initialization:

$$\mathbf{e}^0(\mathbf{x}) = 0, \quad \boldsymbol{\sigma}^0(\mathbf{x}) = \mathbf{L}(\mathbf{x}) : [\mathbf{E} + x_3\boldsymbol{\chi} + \mathbf{e}^0(\mathbf{x})],$$

Iterate $i+1$: $\mathbf{e}^i(\mathbf{x})$ and $\boldsymbol{\sigma}^i(\mathbf{x})$ being known

$$\begin{aligned}
&\text{(a)} \quad \boldsymbol{\tau}^i(\mathbf{x}) = \boldsymbol{\sigma}^i(\mathbf{x}) - \mathbf{L}^o : \mathbf{e}^i(\mathbf{x}),\\
&\text{(b)} \quad \hat{\boldsymbol{\tau}}^i(\mathbf{k}) = \mathscr{F}_3[\boldsymbol{\tau}^i(\mathbf{x})],\\
&\text{(c)} \quad \hat{\mathbf{e}}_p^{i+1}(\mathbf{k}) = -\widehat{\boldsymbol{\Gamma}}(\mathbf{k}) : \hat{\boldsymbol{\tau}}^i(\mathbf{k}) \quad \forall \mathbf{k}\neq 0, \quad \hat{\mathbf{e}}_p^{i+1}(0) = 0 \quad \text{and} \quad \tilde{\mathbf{e}}_h^{i+1}(\tilde{\mathbf{k}}, x_3),\\
&\text{(d)} \quad \mathbf{e}_p^{i+1}(\mathbf{x}) = \mathscr{F}_3^{-1}[\hat{\mathbf{e}}_p^{i+1}(\mathbf{k})] \quad \text{and} \quad \mathbf{e}_h^{i+1}(\mathbf{x}) = \mathscr{F}_2^{-1}[\tilde{\mathbf{e}}_h^{i+1}(\tilde{\mathbf{k}}, x_3)],\\
&\text{(e)} \quad \mathbf{e}^{i+1}(\mathbf{x}) = \mathbf{e}_p^{i+1}(\mathbf{x}) + \mathbf{e}_h^{i+1}(\mathbf{x}),\\
&\text{(f)} \quad \boldsymbol{\sigma}^{i+1}(\mathbf{x}) = \mathbf{L}(\mathbf{x}) : [\mathbf{E} + x_3\boldsymbol{\chi} + \mathbf{e}^{i+1}(\mathbf{x})],\\
&\text{(g)} \quad \text{Convergence test,}
\end{aligned} \tag{40}$$

where $\mathscr{F}_l$ and $\mathscr{F}_l^{-1}$ denote the Fourier transform and its inverse. Subscript l denotes the number of dimensions needed for the Fourier transform. Additionally, the periodic strain fields $(\mathbf{e}^p(\mathbf{x}), \hat{\mathbf{e}}^p(\mathbf{k}))$ are computed by the FFT algorithm in the 3 directions $(\mathscr{F}_3)$ while the complementary fields $(\mathbf{e}^h(\mathbf{x}), \tilde{\mathbf{e}}^h(\tilde{\mathbf{k}}, x_3))$ need only the Fourier transformations along the 2 periodic directions of the plate $(\mathscr{F}_2)$. The explicit calculation of the strains $\tilde{\mathbf{e}}^h(\tilde{\mathbf{k}}, x_3)$ is given in the Appendix A.2.

For the convergence test, Moulinec and Suquet (1998) proposed a convergence criterion which ensures that all local equations (and more specifically the equilibrium equations) are accurately satisfied. In practice, this requirement is stronger than the convergence of the elastic energy. However, due to the fact that the effective elastic properties of the plate in this paper

are directly obtained by the consideration of the elastic strain energy as described in Section 3.1, it is logical to choose the energy criterion for the convergence of the algorithm (40). The iterative procedure is stopped at step $i+1$ when the relative increment between step i and step $i+1$ of strain energy is smaller than a prescribed value ς (typically $\varsigma = 10^{-4}$ in our calculations. This value ensures the convergence of the effectives elastic properties of the plate).

4. Numerical applications

Numerical applications of the previous theory are performed for two examples. The first example is the study of a laminate problem. The comparison is made with the closed-form solution. In the second example, we consider a plane problem related to an inclusion which is periodic along one direction of the horizontal plane of the plate. The homogenized stiffnesses obtained are compared to those of a finite element model.

4.1. Laminate

Let us consider a symmetrical laminate which is made of four homogeneous layers having the same thickness. This laminate may be considered as having a periodic structure along direction x (problem 2D) so that it is possible to extract a unit cell presented in Fig. 1. The following parameters are used for numerical computations, $t = 0.1$, $l_1 = 0.1$ and $E_1 = 46$ GPa, $\nu_1 = 0.3$, $E_2 = 10$ GPa, $\nu_2 = 0.3$ (Young's modulus, Poisson's ratio of the phases 1 and 2, respectively).

The effective properties of the plate are obtained by consideration of the strain energy defined in (37). It can be computed by an equivalent way in the Fourier space (see e.g. Soize, 1993). Due to the symmetry with respect to the middle surface, the coupling stiffness of the plate B is null. It is thus sufficient to identify the homogenized stiffnesses (A, D). The macroscopic fields used for the computation are: $(E = 1, \chi = 0)$, $(E = 0, \chi = 1)$. They allow to calculate the homogenized membrane and bending stiffnesses of the plate, respectively. The solution is compared to classical closed-form solutions of the effective stiffnesses of the Love–Kirchhoff plate given by the following relations:

$$A = \sum_{i=1}^{n} (h_i - h_{i-1}) \frac{E_i}{1-\nu_i^2}, \quad B = \frac{1}{2} \sum_{i=1}^{n} (h_i^2 - h_{i-1}^2) \frac{E_i}{1-\nu_i^2}, \quad D = \frac{1}{3} \sum_{i=1}^{n} (h_i^3 - h_{i-1}^3) \frac{E_i}{1-\nu_i^2}, \tag{41}$$

where h_i (i=1,...,5) are the vertical positions of the bottom face, interfaces between the layers, and the top face of the plate, respectively (see Fig. 1).

Table 1 presents the homogenized stiffnesses obtained from the present theory and from the closed-form solution. The values noted in parentheses represent the CPU times when using a standard PC. The results obtained in Table 1 are calculated by using a low number of discretized points along x-direction ($N_1 = 2^3$). That can be explained by the fact that the material properties are uniform in the horizontal plane of the plate. In addition, the results showed that the convergence of the solution toward the closed-form solution is fast so that a good approximation can be reached for a low number of discretization points along the z-direction ($N_3 = 2^6$). The iterative algorithm is stopped after 10 iterations for $\varsigma = 10^{-4}$. Fig. 2 presents the

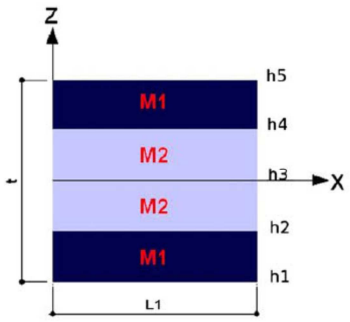

Fig. 1. Elementary cell of 4-layer plate.

Table 1
Effective stiffnesses of the symmetrical 4-layer plate, $N_1 = 2^3$

	Analytical solution	Present solution			
		$N_3 = 2^4$	$N_3 = 2^5$	$N_3 = 2^6$	No. itera.
A	3.0769	3.077 (0.4s)	3.077 (0.7s)	3.077 (1.2s)	10
D	0.0038	0.00382 (0.5s)	0.003805 (0.8s)	0.003802 (1.2s)	10

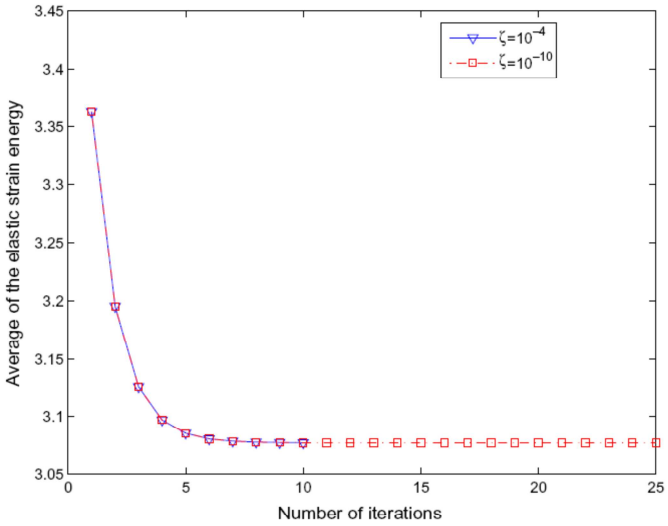

Fig. 2. Convergence of the elastic strain energy.

variation profile of the average of elastic strain energy for the calculation of the membrane stiffness given in Table 1. It can be observed that the strain energy converges rapidly after less than 10 iterations and that the value obtained for $\varsigma = 10^{-4}$ is stable when the iterative process is continued (up to 10^{-10}).

The rate of convergence of the algorithm depends on the following parameters: the wave number N used in the Fourier transforms, the number of iterations during the iterative process, the elastic properties of the reference medium and of the phases. The studies of the convergence of the basic iterative algorithm can be found in Moulinec and Suquet (1994), Moulinec and Suquet (1998), Michel et al. (1999). Improved algorithms for an arbitrary phase contrast are described by Michel et al. (2001) and Moulinec and Suquet (2003). These authors used a convergence criterium based on the vanishing of the local equilibrium equations. In the case of the plate, the local equilibrium does not suffice to insure the equilibrium, because it must be completed by the traction-free boundary condition on the faces of the plate. It is shown above that the energy computed with an accuracy of 1e−4 remains stationary when the convergence process is continued and that the possible occurence of a"plateau" is excluded. Bonnet (2007) considered also the convergence of the basic algorithm for the sum of the Neuman series. For a two-phase composite medium, the Lamé coefficients (λ, μ) of the homogeneous reference medium are related to the properties of the phases by:

$$\begin{aligned} \lambda &= \alpha\lambda_m + (1-\alpha)\lambda_i, \\ \mu &= \alpha\mu_m + (1-\alpha)\mu_i, \end{aligned} \tag{42}$$

where the subscripts m, i denote matrix and inclusion, respectively. For the properties of the reference medium, Michel et al. (1999), Moulinec and Suquet (1994, 1998) used $\alpha = 0.5$ to ensure the convergence of the local fields in the calculations of the basic algorithm. This value has been also used for the computations in the above laminate problem.

4.2. Plate with periodic inclusions

We consider in this section a panel with a periodic repartition of parallelipedic fibers. Fig. 3 presents the 2D section of the panel structure and the corresponding unit cell. The following parameters are used for numerical calculations, $t_1 = 0.025$, $l_1 = 0.1$, $\nu_i = 0.3$, $t_2 = 0.025$, $t = 0.1$, $\nu_m = 0.3$.

As for the case of the laminate, the calculation of the homogenized membrane stiffness of the plate is performed by using the uniform macroscopic strain condition $(E = 1)$, while the computation of the effective bending stiffness is obtained by the condition $(\chi = 1)$. The cell is symmetrical in this example which leads obviously to null coupling stiffness. The approximate solution of the present model is validated by comparison with that of a finite element model. The finite element calculation is performed with a meshing which ensures the convergence of the elastic strain energy. The solution is obtained by using ABAQUS software and linear quadrilateral elements CPE4R (plane strain). Additionally, it can be seen that the periodic cell presents two axes of symmetry. As a consequence, it is sufficient to consider a quarter of the periodic cell (2D problem). Figs. 4 and 5 present the displacement boundary conditions for the calculation of the homogenized stiffnesses A and D, respectively. The boundary conditions taking into account the symmetries of the period are obtained from the developments reported in Appendix B. The measurement of a "relative error" is defined by the relationship:

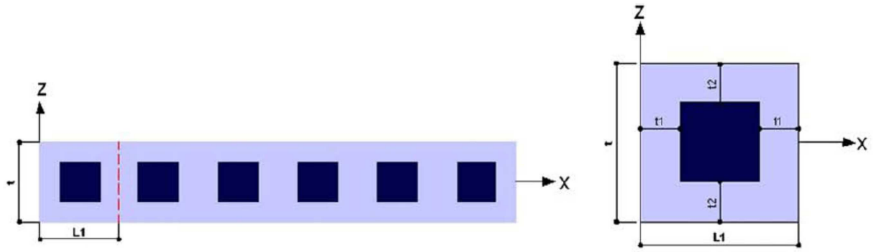

Fig. 3. Panel with periodic inclusions and the related unit cell.

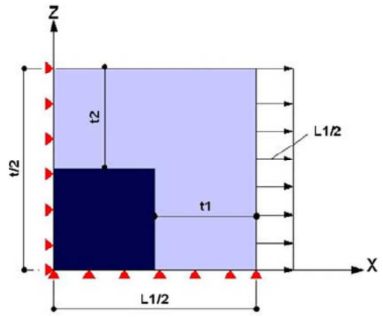

Fig. 4. FEM model: displacement condition on a quarter of unit cell for calculation of *A*.

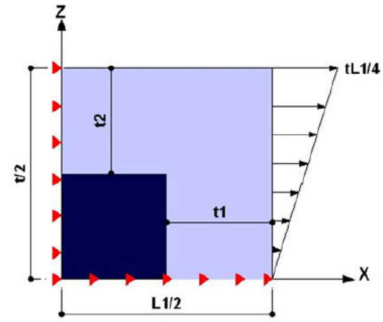

Fig. 5. FEM model: displacement condition on a quarter of unit cell for calculation of *D*.

$$\text{error}\,(\%) = \frac{M_c - M_m}{M_m} \times 100\%, \tag{43}$$

where M_c is the solution obtained from the present model, and M_m is the one obtained from the FEM model.

Tables 2 and 3 provide the comparison between the homogenized stiffnesses *A* and *D* obtained, respectively, by the present theory and by the finite element model. The space discretization defined in (38) is performed by using the same number of points along two directions, i.e. $N_1 = N_3 = N$. It can be seen that the homogenized properties are near to those obtained from the finite element model even for a low number of pixels. The variation profile of the solution in comparison with the FEM solution is presented in Figs. 6 and 7 where it can be seen that the bending stiffness and the membrane stiffness display an opposite variation with the spatial resolution of the image: the bending stiffness decreases with the spatial resolution while the membrane stiffness increases with the spatial resolution. Usually (Moulinec and Suquet,1994, 1998), it is observed that the elastic energy decreases when increasing the spatial resolution in the case of a problem where a macroscopic strain is applied at the beginning of the iterative process. Conversely (Bonnet, 2007), the dual method using an applied macroscopic stress leads to increasing values of the elastic energy. In the present case, a macroscopic strain is applied, but traction-free boundary conditions are taken into account along the boundaries of the plate. The mixed nature of the problem explains the different kinds of convergences observed in Figs. 6 and 7.

Table 2
Effective membrane stiffness of the panel plate, $E_i/E_m = 10, E_m = 1, \alpha = 0.5$

N	FEM	Proposed solution		
		Value (error %)	Times (s)	No. itera.
2^4	0.16288	0.16209 (−0.485%)	0.9	15
2^5	0.16288	0.16257 (−0.19%)	3.4	16
2^6	0.16288	0.16279 (−0.055%)	12	16
2^7	0.16288	0.16287 (−0.006%)	50	16

Table 3
Effective bending stiffness of the panel plate, $E_i/E_m = 10, E_m = 1, \alpha = 0.5$

N	FEM	Proposed solution		
		Value (error %)	Times (s)	No. itera.
2^4	1.0652e−4	1.0701e−4 (0.460%)	1	18
2^5	1.0652e−4	1.0659e−4 (0.066%)	4	18
2^6	1.0652e−4	1.0654e−4 (0.019%)	14	18
2^7	1.0652e−4	1.0654e−4 (0.019%)	57	18

The reference medium is chosen according to Michel et al. (1999), Moulinec and Suquet (1994, 1998) with $\alpha = 0.5$. The CPU times and the number of iterations depend on the contrast between the phases and on the discretized number of points. As seen in Tables 2 and 3 the calculation time for the problem with contrast $E_i/E_m = 10$ and stiffer inclusions increases with the number of discretization points. In practice, a difficulty of convergence was observed by other authors when using the present basic algorithm for composites with very stiff inclusions (Moulinec and Suquet,1994, 1998; Michel et al., 1999; Bonnet, 2007). The accelerated scheme of Eyre and Milton (1999), the augmented Lagrangian method of Michel et al. (2001) or the dual solution (stress formulation) described in Bonnet (2007) could be considered to obtain a better convergence in this case.

Solutions for inclusions softer than the matrix or voids are also reported here, for which the parameter $\alpha = 0.65$ proposed by Bonnet (2007) has been used. Tables 4 and 5 present the comparison between the homogenized membrane and bending stiffnesses of the plate obtained from the present model and from the FEM model. The solutions are obtained for a contrast $E_m/E_i = 1000$. It can be seen that the homogenized stiffnesses obtained from the present solution agree with those of the FEM even for a low resolution. The iterative procedure is stopped after about 8 iterations for a prescribed value of the relative error of 10^{-4}. Additionally, the CPU times obtained in Tables 4 and 5 show the fastness of computation.

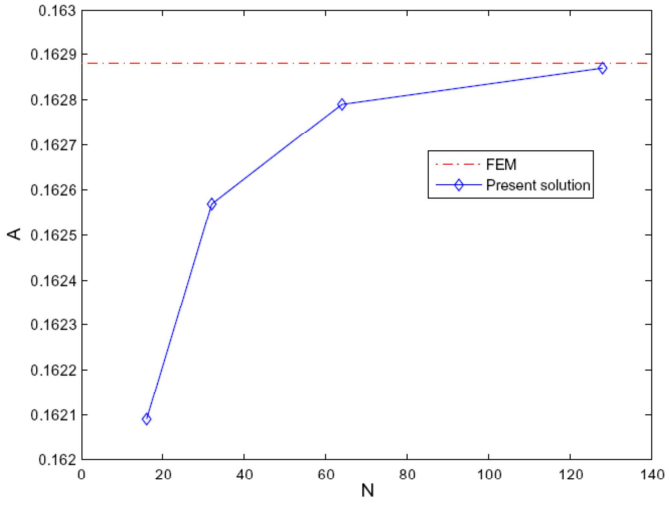

Fig. 6. Comparison for A with the FEM solution.

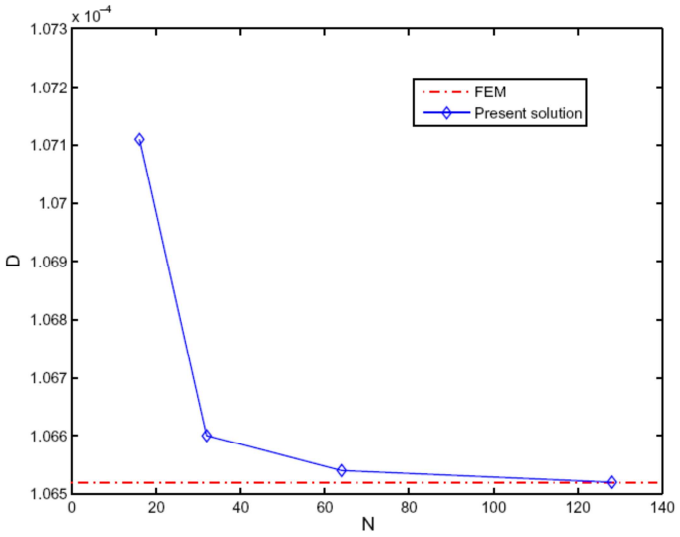

Fig. 7. Comparison for D with the FEM solution.

Table 4
Effective membrane stiffness of the panel plate, $E_m/E_i = 1000, E_i = 1, \alpha = 0.65$

N	FEM	Present solution		
		Value (relative error %)	Times (s)	No. itera.
2^4	58.495	58.363 (−0.226%)	0.6	8
2^5	58.495	58.472 (−0.039%)	2	9
2^6	58.495	58.502 (0.0120%)	7	9
2^7	58.495	58.506 (0.0188%)	28	9

Table 5
Homogenized bending stiffness of the panel plate, $E_m/E_i = 1000, E_i = 1, \alpha = 0.65$

N	FEM	Present solution		
		Value (relative error %)	Times (s)	No. itera.
2^4	0.08225	0.08244 (0.231%)	0.5	8
2^5	0.08225	0.08230 (0.060%)	1.7	8
2^6	0.08225	0.08227 (0.024%)	6	8
2^7	0.08225	0.08226 (0.012%)	25	8

Table 6
Homogenized membrane stiffness of the panel plate, $E_i = 0, E_m = 10$

N	FEM	Present solution		
		Value (relative error %)	Times (s)	No. itera.
2^4	0.5840	0.5826 (−0.24%)	0.6	8
2^5	0.5840	0.5837 (−0.05%)	2	9
2^6	0.5840	0.5839 (−0.017%)	7	9
2^7	0.5840	0.5840 (∼ 0.0%)	28	9

For the plate with a periodic rectangular void, Tables 6 and 7 present the comparison of the effective stiffnesses with those obtained by FEM. Elastic moduli $E_i = 0$, $E_m = 10$GPa are chosen for the computations. As previously, the results provide a good precision even for a low resolution. The CPU time increases with the number of discretization points, but it can be seen that in spite of the infinite contrast between voids and matrix, the iterations are stopped rapidly when the iterative scheme is stopped for a prescribed relative error of 10^{-4} (see Tables 6 and 7).

Table 7
Homogenized bending stiffness of the panel plate, $E_i = 0, E_m = 10$

N	FEM	Present solution		
		Value (relative error %)	Times (s)	No. itera.
2^4	8.224e−4	8.242e−4 (0.219%)	0.6	8
2^5	8.224e−4	8.228e−4 (0.049%)	2	8
2^6	8.224e−4	8.225e−4 (0.012%)	6	8
2^7	8.224e−4	8.224e−4 (∼ 0.0%)	25	8

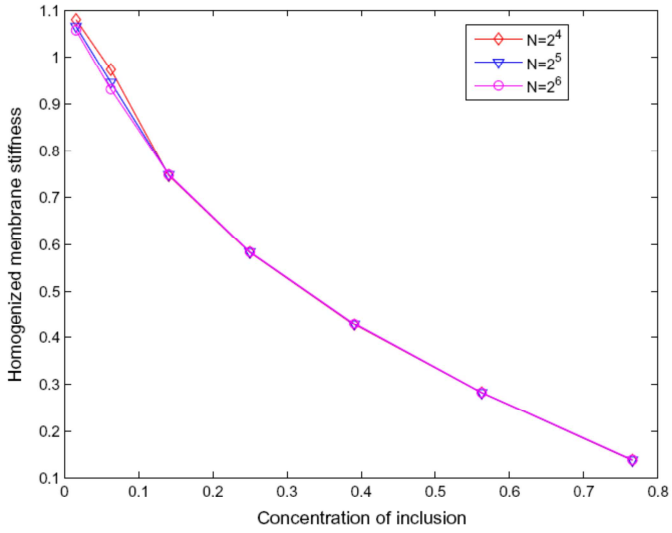

Fig. 8. Variation of the membrane stiffness according to the volume fraction of inclusion.

To check the validity of the present solution for different volume fractions of voids, Figs. 8 and 9 present the homogenized stiffnesses of the plate in terms of the concentration of voids (the volume fraction of voids varies within $[1/64, 49/64]$) and of the number of discretized points in one direction N. As for the results obtained in Tables 6 and 7 it can be seen that a number of wave-numbers of $N = 2^5$ in each direction is convenient to reach the convergence.

5. Conclusion

This paper has presented a $\boldsymbol{\Gamma}$-operator for the media with mixed boundary conditions: periodicity conditions and traction-free boundary conditions. This operator computed from the properties of a "reference medium" has been used to obtain the solution on the cell period needed to obtain the effective properties of plates made of periodically distributed inhomogeneous cells. Applications were performed and the comparison of the results obtained here with those obtained from closed-form solutions and with finite element results have shown the accuracy and the speed of convergence of the series solution. The convergence is slow for very stiff inclusions. The solution could be improved by using the accelerated scheme of Eyre and Milton (1999), the augmented Lagrangian method of Michel et al. (2001) or the dual solution (stress formulation) described in Bonnet (2007). The numerical computations reported in this paper have been performed for 2D-case. The application of the method described in this paper to 3D problems increases the quantity of wave numbers by $N^{3/2}$. However, the high speed of the Fourier method can allow this increase of computational cost.

Appendix A. Solution of the complementary problem

A.1. Displacement field

The complementary solution $\tilde{\mathbf{u}}^h(\tilde{\mathbf{k}}, x_3)$ is obtained from a second order differential equation system with 3 degrees of freedom which was described in (23) and (24). To solve this problem, the solution field is chosen of the form:

$$\tilde{\mathbf{u}}^h(\tilde{\mathbf{k}}, x_3) = \mathbf{d}\, e^{rx_3}, \quad \mathbf{d} \neq 0. \tag{A.1}$$

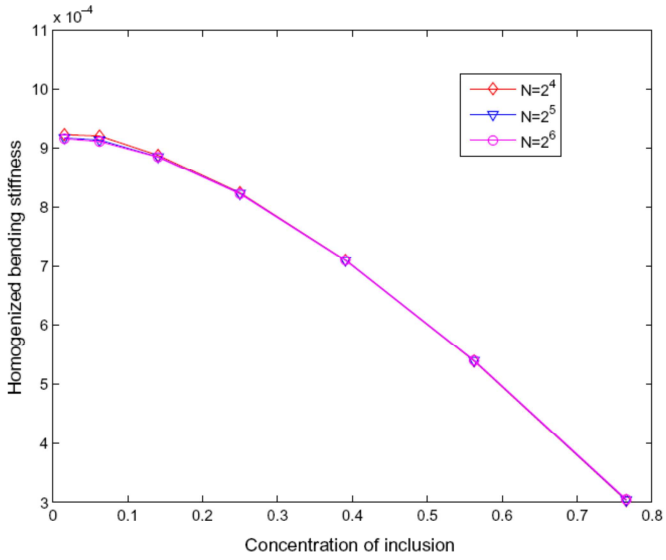

Fig. 9. Variation of the bending stiffness according to the volume fraction of inclusion.

Substituting this field into the system (23) leads to the following condition, deduced from the null value of the determinant of the system of equations:

$$(r^2 - s^2)^3 = 0 \quad \text{where } s = \sqrt{k_1^2 + k_2^2}. \tag{A.2}$$

Generally, this relation leads a priori to the fact that $\mathbf{d}$ is a second-order polynomial of x_3 and that the solution is of the form:

$$\tilde{\mathbf{u}}^h(\tilde{\mathbf{k}}, x_3) = (\mathbf{a}^+ + \mathbf{b}^+ x_3 + \mathbf{c}^+ x_3^2)\, e^{sx_3} + (\mathbf{a}^- + \mathbf{b}^- x_3 + \mathbf{c}^- x_3^2)\, e^{-sx_3}. \tag{A.3}$$

However, the values of $(\mathbf{a}^{\pm}, \mathbf{b}^{\pm}, \mathbf{c}^{\pm})$ are not independent, because the solution of the system of Eq. (23) must be described by using only 6 independent constants. Introducing expression (A.3) into Eq. (23) allows to express $\tilde{\mathbf{u}}^h$ by using 6 independent constants $a_1^+, a_1^-, a_2^+, a_2^-, b_3^+, b_3^-$ and to show that $\mathbf{c}^+ = \mathbf{c}^- = 0$.

More precisely, the three boundary conditions at the top face $(x_3 = t/2)$ and the three boundary conditions at the bottom face $(x_3 = -t/2)$ of the unit cell enable the construction of a system of six equations for determining six coefficients of the vector $\xi = (a_1^+, a_1^-, a_2^+, a_2^-, b_3^+, b_3^-)$.

$$\mathbf{K}\boldsymbol{\xi} = \mathbf{q} \tag{A.4}$$

where:

$$\mathbf{K} = \begin{bmatrix}
(s^2+k_1^2)e^{s\frac{t}{2}} & -(s^2+k_1^2)e^{-s\frac{t}{2}} & k_1k_2e^{s\frac{t}{2}} & -k_1k_2e^{-s\frac{t}{2}} & 2ik_1\left(s\frac{t}{2}-\frac{\mu}{\lambda+\mu}\right)e^{s\frac{t}{2}} & 2ik_1\left(s\frac{t}{2}+\frac{\mu}{\lambda+\mu}\right)e^{-s\frac{t}{2}} \\
(s^2+k_1^2)e^{-s\frac{t}{2}} & -(s^2+k_1^2)e^{s\frac{t}{2}} & k_1k_2e^{-s\frac{t}{2}} & -k_1k_2e^{s\frac{t}{2}} & -2ik_1\left(s\frac{t}{2}+\frac{\mu}{\lambda+\mu}\right)e^{-s\frac{t}{2}} & -2ik_1\left(s\frac{t}{2}-\frac{\mu}{\lambda+\mu}\right)e^{s\frac{t}{2}} \\
k_1k_2e^{s\frac{t}{2}} & -k_1k_2e^{-s\frac{t}{2}} & (s^2+k_2^2)e^{s\frac{t}{2}} & -(s^2+k_2^2)e^{-s\frac{t}{2}} & 2ik_2\left(s\frac{t}{2}-\frac{\mu}{\lambda+\mu}\right)e^{s\frac{t}{2}} & 2ik_2\left(s\frac{t}{2}+\frac{\mu}{\lambda+\mu}\right)e^{-s\frac{t}{2}} \\
k_1k_2e^{-s\frac{t}{2}} & -k_1k_2e^{s\frac{t}{2}} & (s^2+k_2^2)e^{-s\frac{t}{2}} & -(s^2+k_2^2)e^{s\frac{t}{2}} & -2ik_2\left(s\frac{t}{2}+\frac{\mu}{\lambda+\mu}\right)e^{-s\frac{t}{2}} & -2ik_2\left(s\frac{t}{2}-\frac{\mu}{\lambda+\mu}\right)e^{s\frac{t}{2}} \\
-2\mu ik_1e^{s\frac{t}{2}} & -2\mu ik_1e^{-s\frac{t}{2}} & -2\mu ik_2e^{s\frac{t}{2}} & -2\mu ik_2e^{-s\frac{t}{2}} & 2\mu\left(s\frac{t}{2}-\frac{\lambda+2\mu}{\lambda+\mu}\right)e^{s\frac{t}{2}} & -2\mu(s\frac{t}{2}+\frac{\lambda+2\mu}{\lambda+\mu})e^{-s\frac{t}{2}} \\
-2\mu ik_1e^{-s\frac{t}{2}} & -2\mu ik_1e^{s\frac{t}{2}} & -2\mu ik_2e^{-s\frac{t}{2}} & -2\mu ik_2e^{s\frac{t}{2}} & -2\mu\left(s\frac{t}{2}+\frac{\lambda+2\mu}{\lambda+\mu}\right)e^{-s\frac{t}{2}} & 2\mu\left(s\frac{t}{2}-\frac{\lambda+2\mu}{\lambda+\mu}\right)e^{s\frac{t}{2}}
\end{bmatrix}, \tag{A.5}$$

and the components of the vector $\mathbf{q} = (q_1^+, q_1^-, q_2^+, q_2^-, q_3^+, q_3^-)$ are defined in (29). The closed-form solution of (A.4) is given by (28) and (29).

A.2. Strain field

The calculation of the strain field $\tilde{\mathbf{e}}^h(\tilde{\mathbf{k}}, x_3)$ for $|\tilde{\mathbf{k}}| \neq 0$ is performed owing to the compatibility condition (21) which may be expressed as follows:

$$\tilde{\mathbf{e}}^h(\tilde{\mathbf{k}}, x_3) = \mathbf{P}(\tilde{\mathbf{k}}, x_3) \cdot \xi(\tilde{\mathbf{k}}), \quad \forall |\tilde{\mathbf{k}}| \neq 0 \, (s \neq 0), \tag{A.6}$$

where:

$$\mathbf{P} = \begin{bmatrix} \mathrm{i}k_1 \mathrm{e}^{sx_3} & \mathrm{i}k_1 \mathrm{e}^{-sx_3} & 0 & 0 & -\frac{k_1^2}{s} x_3 \mathrm{e}^{sx_3} & \frac{k_1^2}{s} x_3 \mathrm{e}^{-sx_3} \\ 0 & 0 & \mathrm{i}k_2 \mathrm{e}^{sx_3} & \mathrm{i}k_2 \mathrm{e}^{-sx_3} & -\frac{k_2^2}{s} x_3 \mathrm{e}^{sx_3} & \frac{k_2^2}{s} x_3 \mathrm{e}^{-sx_3} \\ -\mathrm{i}k_1 \mathrm{e}^{sx_3} & -\mathrm{i}k_1 \mathrm{e}^{-sx_3} & -\mathrm{i}k_2 \mathrm{e}^{sx_3} & -\mathrm{i}k_2 \mathrm{e}^{-sx_3} & \left(x_3 s - \frac{2\mu}{\lambda+\mu}\right) \mathrm{e}^{sx_3} & -\left(x_3 s + \frac{2\mu}{\lambda+\mu}\right) \mathrm{e}^{-sx_3} \\ \frac{k_1 k_2}{2s} \mathrm{e}^{sx_3} & -\frac{k_1 k_2}{2s} \mathrm{e}^{-sx_3} & \frac{s^2+k_2^2}{2s} \mathrm{e}^{sx_3} & -\frac{s^2+k_2^2}{2s} \mathrm{e}^{-sx_3} & \frac{\mathrm{i}k_2}{s} (x_3 s - \frac{\mu}{\lambda+\mu}) \mathrm{e}^{sx_3} & \frac{\mathrm{i}k_2}{s} (x_3 s + \frac{\mu}{\lambda+\mu}) \mathrm{e}^{-sx_3} \\ \frac{s^2+k_1^2}{2s} \mathrm{e}^{sx_3} & -\frac{s^2+k_1^2}{2s} \mathrm{e}^{-sx_3} & \frac{k_1 k_2}{2s} \mathrm{e}^{sx_3} & -\frac{k_1 k_2}{2s} \mathrm{e}^{-sx_3} & \frac{\mathrm{i}k_1}{s} \left(x_3 s - \frac{\mu}{\lambda+\mu}\right) \mathrm{e}^{sx_3} & \frac{\mathrm{i}k_1}{s} \left(x_3 s + \frac{\mu}{\lambda+\mu}\right) \mathrm{e}^{-sx_3} \\ \frac{\mathrm{i}k_2}{2} \mathrm{e}^{sx_3} & \frac{\mathrm{i}k_2}{2} \mathrm{e}^{-sx_3} & \frac{\mathrm{i}k_1}{2} \mathrm{e}^{sx_3} & \frac{\mathrm{i}k_1}{2} \mathrm{e}^{-sx_3} & -\frac{k_1 k_2}{s} x_3 \mathrm{e}^{sx_3} & \frac{k_1 k_2}{s} x_3 \mathrm{e}^{-sx_3} \end{bmatrix}. \tag{A.7}$$

For $|\tilde{\mathbf{k}}| = 0$, the membrane strains $\tilde{e}^h_{\alpha\beta}$ are null due to the periodicity on ∂Y_l of the displacement field, i.e. $\tilde{e}^h_{\alpha\beta}(\tilde{\mathbf{k}} = 0, x_3) = 0$. The calculation of $\tilde{e}^h_{\beta 3}(\tilde{\mathbf{k}} = 0, x_3)$ is also performed by using the boundary condition (27) and the differential system of Eq. (23). This gives the components of the out-of-plane strain field as follows:

$$\begin{aligned} \tilde{e}^h_{33}(\tilde{\mathbf{k}} = 0, x_3) &= -\frac{1}{\lambda + 2\mu} \sum_{k_3} \hat{\sigma}^p_{33}(\tilde{\mathbf{k}} = 0, k_3) \, \mathrm{e}^{\mathrm{i}k_3 \frac{t}{2}} \\ \tilde{e}^h_{\alpha 3}(\tilde{\mathbf{k}} = 0, x_3) &= -\frac{1}{2\mu} \sum_{k_3} \hat{\sigma}^p_{\alpha 3}(\tilde{\mathbf{k}} = 0, k_3) \, \mathrm{e}^{\mathrm{i}k_3 \frac{t}{2}}, \quad \alpha = 1, 2. \end{aligned} \tag{A.8}$$

Appendix B. Modelling a periodic symmetrical cell

The symmetries enable to obtain simplifications, more specifically concerning the boundary conditions. The symmetries lead indeed to the use of "Dirichlet" boundary conditions instead of "periodicity" conditions, the former ones being easier to account for within finite element computations (see Cecchi and Sab, 2002b). Let us consider a symmetrical periodic cell Y which is subjected to the boundary conditions (33). The symmetrical domain Y is defined as follows:

$$Y = \left]-\frac{l_1}{2}, \frac{l_1}{2}[\times]-\frac{l_2}{2}, \frac{l_2}{2}[\times]-\frac{t}{2}, \frac{t}{2}\right[.$$

In a general way, if $\mathbf{x} \to \mathbf{u}^*(\mathbf{x})$ is the image of the displacement field $\mathbf{x} \to \mathbf{u}(\mathbf{x})$ by a symmetry $\mathbf{S}$, we have:

$$\mathbf{u}^*(\mathbf{x}) = \mathbf{S} \cdot \mathbf{u}({}^t\mathbf{S} \cdot \mathbf{x}),$$

while the image of a second order tensor by the symmetry $\mathbf{S}$ is expressed as follows:

$$\mathbf{M}^*(\mathbf{x}) = \mathbf{S} \cdot \mathbf{M}({}^t\mathbf{S} \cdot \mathbf{x}) \cdot {}^t\mathbf{S}.$$

These calculations imply that the image by $\mathbf{S}$ of the solution $(\boldsymbol{\sigma}, \boldsymbol{\epsilon}, \mathbf{u})$ of the problem (32) and (33) complies to the following system:

$$\begin{cases} \boldsymbol{\sigma}^* \cdot \nabla = 0, \quad \boldsymbol{\sigma}^*(\mathbf{x}) = \mathbf{L}(\mathbf{x}) : \boldsymbol{\epsilon}^*(\mathbf{x}), \\ \boldsymbol{\epsilon}^*(x) = \mathbf{S} \cdot \mathbf{E}({}^t\mathbf{S} \cdot \mathbf{x}) \cdot {}^t\mathbf{S} + (\mathbf{S} \cdot \mathbf{x})_3 \mathbf{S} \cdot \boldsymbol{\chi}({}^t\mathbf{S} \cdot \mathbf{x}) \cdot {}^t\mathbf{S} + \mathbf{S} \cdot \mathbf{e}({}^t\mathbf{S} \cdot \mathbf{x}) \cdot {}^t\mathbf{S}, \\ \sigma^*_{j3} = 0 \quad \text{on} \quad \partial Y^{\pm}, \\ \mathbf{u}^*(\mathbf{x}) \text{ periodic on } \partial Y_l, \quad \boldsymbol{\sigma}^*(\mathbf{x}) \text{ antiperiodic on } \partial Y_l, \end{cases} \tag{B.1}$$

where the elastic coefficients of $\mathbf{L}(\mathbf{x})$ are assumed to be left invariant by the symmetry $\mathbf{S}$. It can be seen that if a symmetry $\mathbf{S}$ and macroscopic tensors $(\mathbf{E}, \boldsymbol{\chi})$ are chosen so that,

$$\begin{cases} \mathbf{E}(\mathbf{x}) = \mathbf{S} \cdot \mathbf{E}({}^t\mathbf{S} \cdot \mathbf{x}) \cdot {}^t\mathbf{S}, \\ x_3 \boldsymbol{\chi}(\mathbf{x}) = (\mathbf{S} \cdot \mathbf{x})_3 \mathbf{S} \cdot \boldsymbol{\chi}({}^t\mathbf{S} \cdot \mathbf{x}) \cdot {}^t\mathbf{S}, \end{cases} \tag{B.2}$$

the star and non-star variables will comply to the same system of equations. It remains to check that these variables are subjected to the same boundary conditions. In this appendix, it will be shown how to take into account the symmetry for two cases of the plane problem: $(\mathbf{E} = 1, \boldsymbol{\chi} = 0)$ and $(\mathbf{E} = 0, \boldsymbol{\chi} = 1)$.

For the first case ($\mathbf{E}=1$, $\boldsymbol{\chi}=0$), the matrix $\mathbf{S}$ corresponding to the symmetry with respect to the z-axis is of the form:

$$\mathbf{S}=\begin{pmatrix}-1 & 0\\ 0 & 1\end{pmatrix}. \tag{B.3}$$

By using the symmetry properties, the images of the fields $(\boldsymbol{\sigma},\boldsymbol{\epsilon},\mathbf{u})$ by the symmetry $\mathbf{S}$ are obtained by the following expressions:

$$\mathbf{u}^*(x,z)=\begin{Bmatrix}-u_x(-x,z)\\ u_z(-x,z)\end{Bmatrix},\quad \mathbf{e}^*(x,z)=\begin{pmatrix}e_{xx} & -e_{xz}\\ -e_{xz} & e_{zz}\end{pmatrix}(-x,z), \tag{B.4}$$

$$\boldsymbol{\sigma}^*(x,z)=\begin{pmatrix}\sigma_{xx} & -\sigma_{xz}\\ -\sigma_{xz} & \sigma_{zz}\end{pmatrix}(-x,z). \tag{B.5}$$

It can be seen in this case that the symmetry relative to the z-axis complies to the relationship (B.2). It means that $\mathbf{u}^*$ and $\mathbf{u}$ comply to the same field equations and to the same boundary conditions. The images $\mathbf{u}^*$ and $\boldsymbol{\sigma}^*$ are therefore also a solution of the problem. Taking into account the periodicity conditions of the displacement field and the antiperiodicity conditions of the stress field on ∂Y_l leads to:

$$\begin{aligned}&u_x(0,z)=u_x\left(\frac{l_1}{2},z\right)=u_x\left(-\frac{l_1}{2},z\right)=0,\\ &\sigma_{xz}(0,z)=\sigma_{xz}\left(\frac{l_1}{2},z\right)=\sigma_{xz}\left(-\frac{l_1}{2},z\right)=0.\end{aligned} \tag{B.6}$$

If the symmetry with respect to the x-axis is considered, the symmetrical matrix $\mathbf{S}$ is given by:

$$\mathbf{S}=\begin{pmatrix}1 & 0\\ 0 & -1\end{pmatrix}. \tag{B.7}$$

The images of the fields $(\boldsymbol{\sigma},\boldsymbol{\epsilon},\mathbf{u})$ are then obtained:

$$\mathbf{u}^*(x,z)=\begin{Bmatrix}u_x(x,-z)\\ -u_z(x,-z)\end{Bmatrix},\quad \mathbf{e}^*(x,z)=\begin{pmatrix}e_{xx} & -e_{xz}\\ -e_{xz} & e_{zz}\end{pmatrix}(x,-z), \tag{B.8}$$

$$\boldsymbol{\sigma}^*(x,z)=\begin{pmatrix}\sigma_{xx} & -\sigma_{xz}\\ -\sigma_{xz} & \sigma_{zz}\end{pmatrix}(x,-z). \tag{B.9}$$

It can be observed that the relation (B.2) is always verified, leading to the following boundary conditions:

$$\begin{aligned}&\sigma_{xz}(x,0)=\sigma_{xz}\left(x,-\frac{t}{2}\right)=\sigma_{xz}\left(x,\frac{t}{2}\right)=0,\\ &u_z(x,0)=\sigma_{zz}\left(x,-\frac{t}{2}\right)=\sigma_{zz}\left(x,\frac{t}{2}\right)=0.\end{aligned} \tag{B.10}$$

If the quarter $Y_{1/4}$ of the domain Y is considered, with $Y_{1/4}=\left]0,\frac{l_1}{2}\right[\times\left]0,\frac{t}{2}\right[$, the local boundary value problem for the first case can be solved under the following boundary conditions:

$$\begin{cases}u_x^{\text{total}}(0,z)=\sigma_{xz}(0,z)=\sigma_{xz}\left(\frac{l_1}{2},z\right)=0,\quad u_x^{\text{total}}\left(\frac{l_1}{2},z\right)=\frac{l_1}{2},\\ u_z^{\text{total}}(x,0)=\sigma_{xz}(x,0)=\sigma_{xz}(x,\frac{t}{2})=\sigma_{zz}(x,\frac{t}{2})=0.\end{cases} \tag{B.11}$$

For the second case ($\mathbf{E}=0,\boldsymbol{\chi}=1$), if we consider the symmetry relative to the z-axis, the expression (B.2) is verified. As a result, the boundary conditions defined in (B.6) are used. On the contrary, if we analyze the symmetry relative to the x-axis, the image of the out-of-plane macroscopic strain is defined by $\boldsymbol{\chi}^*=-\mathbf{S}\boldsymbol{\chi}\mathbf{S}$. As a consequence, it can be observed that the fields $-\mathbf{u}^*$ and $-\boldsymbol{\sigma}^*$ are also the solution fields of the problem. It can therefore be deduced that:

$$\begin{aligned}&u_x(x,0)=\sigma_{xz}(x,-\tfrac{t}{2})=\sigma_{xz}(x,\tfrac{t}{2})=0,\\ &\sigma_{zz}(x,0)=\sigma_{zz}(x,-\tfrac{t}{2})=\sigma_{zz}(x,\tfrac{t}{2})=0.\end{aligned} \tag{B.12}$$

Using (B.6) and (B.12), the boundary conditions on the $Y_{1/4}$ can be written by the following expressions:

$$\begin{cases}u_x^{\text{total}}(0,z)=\sigma_{xz}(0,z)=\sigma_{xz}\left(\frac{l_1}{2},z\right)=0,\quad u_x^{\text{total}}\left(\frac{l_1}{2},z\right)=\frac{l_1}{2}z,\\ u_x^{\text{total}}(x,0)=\sigma_{zz}(x,0)=\sigma_{xz}(x,\frac{t}{2})=\sigma_{zz}(x,\frac{t}{2})=0.\end{cases} \tag{B.13}$$

By applying the boundary conditions on the total displacement field $\mathbf{u}^{\text{total}}$ defined in (B.11 and B.13) (for the plane problems), the boundary value problem (32 and 33) can be solved by using a standard finite element package, because it involves now only Dirichlet boundary conditions and no more periodicity conditions. The homogenized properties of the plate can therefore be determined from the strain energy as described in Section 3.1.

References

Auriault, J.L., Bonnet, G., 1985. Dynamique des composites élastiques périodiques. Arch. Mech. 37, 269–284.

Bakhvalov, N.S., Panasenko, G.P., 1989. Homogenization: Averaging Processes in Periodic Media. Kluwer Academic Publishers, Dordrecht, Boston, London.

Bakhvalov, N.S., 1974. Averaged characteristics of bodies with periodic structure (Russian). Dokl. Akad. Nauk. SSSR. 218, 1046–1048.

Bensoussan, A., Lions, J.L., Papanicolaou, G., 1978. Asymptotic analysis for periodic structures. North-Holland, Amsterdam.

Böhm, H.J., Rammerstorfer, F.G., Weissenbek, E., 1993. Some simple models for micromechanical investigations of fiber arrangement effects in MMCs. Comput. Mater. Sci. 1, 177–194.

Bonnet, G., 2007. Effectives properties of elastic periodic composite media with fibers. J. Mech. Phys. Solids 55, 881–899.

Bornert, M., Bretheau, T., Gilormini, P., 2001. Homogénéisation en mécanique des matériaux 1: Matériaux aléatoires élastiques et milieux périodiques. Hermes Science Publications, Paris.

Bourgeois, S., Débordes, O., Patou, P., 1998. Homogénéisation et plasticité des plaques minces. Rev. Eur. Elem. Finis. 7, 39–54.

Brockenbrough, J.R., Suresh, S., Wienecke, H.A., 1991. Deformation of metal-matrix composites with continuous fibers: geometrical effects of fiber distribution and shape. Acta Metall. Mater. 39, 735–752.

Caillerie, D., 1984. Thin elastic and periodic plates. Math. Meth. Appl. Sci. 6, 159–191.

Cecchi, A., Sab, K., 2002a. A multi-parameter homogenization study for modelling elastic masonry. Euro. J. Mech. A/Solids 21, 249–268.

Cecchi, A., Sab, K., 2002b. Out of plane model for heterogenous periodic materials: the case of masonry. Euro. J. Mech. A/Solids 21, 715–746.

Cecchi, A., Sab, K., 2004. A comparison between a 3D discrete model and two homogenized plate models for periodic elastic brickword. Int. J. Solids Struct. 41, 2259–2276.

Cohen, I., Bergman, D.J., 2003. Effective elastic properties of periodic composite medium. J. Mech. Phys. Solids 51, 1433–1457.

Dallot, J., Sab, K., 2008b. Limit analysis of multi-layered plates. Part I: The homogenized Love–Kirchhoff model. J. Mech. Phys. Solids 56, 581–612.

Dallot, J., Sab, K., 2008a. Limit analysis of multi-layered plates.. J. Mech. Phys. Solids 56, 561–580.

Duvaut, G., Metellus, A.M., 1976. Homogénéisation d'une plaque mince en flexion périodique et symétrique. C.R. Acad. Sci. Paris A 283, 947–950.

Eyre, D.J., Milton, G.W., 1999. A fast numerical scheme for computing the response of composites using grid refinement. Eur. Phys. J. AP. 6, 41–47.

Gasquet, C., Witomski, P., 2000. Analyse de Fourier et Applications. Masson, Paris.

Gusev, A.A., 1997. Representative volume element size for elastic composites: a numerical study. J. Mech. Phys. Solids 45, 1449–1459.

Iwakuma, T., Nemat-Nasser, S., 1983. Composites with periodic microstructure. Comput. Struct. 16, 13–19.

Kaßbohm, S., Müller, W.H., Feßler, R., 2005. Fourier series for computing the response of periodic structures with arbitrary stiffness distribution. Comput. Mater. Sci. 32, 387–391.

Kaßbohm, S., Müller, W.H., Feßler, R., 2006. Improved approximations of Fourier coefficients for computing the response of periodic structures with arbitrary stiffness distribution. Comput. Mater. Sci. 37, 90–93.

Kohn, R., Vogelius, M., 1984. A new model for thin plates with rapidly varying thickness. Int. J. Solids Struct. 20, 333–350.

Kröner, E., 1971. Statistical Continuum Mechanics. Springer Verlag, Wien.

Lewiński, T., Telega, J.J., 1999. Plates, Laminates and Shells: Asymptotic Analysis and Homogenization. World Scientific, Publishing, Singapore.

Luciano, R., Barbero, E.J., 1994. Formulas for the stiffness of composites with periodic microstructure. Int. J. Solids Struct. 31, 2933–2944.

Michel, J.C., Moulinec, H., Suquet, P., 1999. Effective properties of composite materials with periodic microstructure: a computational approach. Compu. Meth. Appl. Mech. Eng. 172, 109–143.

Michel, J.C., Moulinec, H., Suquet, P., 2001. A computational scheme for linear and non-linear composites with arbitrary phase contrast. Int. J. Numer. Meth. Eng. 52, 139–160.

Milton, G.W., 2002. The Theory of Composites. Cambridge University Press, Cambridge.

Moulinec, H., Suquet, P., 1994. A fast numerical method for computing the linear and nonlinear properties of composites. C.R. Acad. Sci. 318, 1417–1423.

Moulinec, H., Suquet, P., 1998. A numerical method for computing the overall response of nonlinear composites with complex microstructure. Compu. Meth. Appl. Mech. Eng. 157, 69–94.

Moulinec, H., Suquet, P., 2003. Comparison of FFT-based methods for computing the response of composites with highly contrasted mechanical properties. Physica B 338, 58–60.

Mura, T., 1991. Micromechanics of Deflects in Solids. Kluwer Academic Publishers..

Neumann, S., Herrmann, K.P., Müller, W.H., 2002. Stress/strain computation in heterogenous bodies with discrete Fourier transforms – different approaches. Compu. Mater. Sci. 25, 151–158.

Neumann, S., Herrmann, K.P., Müller, W.H., 2001. Fourier transforms – an alternative to finite elements for elastic–plastic stress–strain analyses of heterogeneous materials. Acta Mech. 149, 149–160.

Sab, K., Nedjar, B., 2005. Periodization of random media and representative volume element size for linear composites. C. R. Mécanique 333, 187–195.

Sab, K., 2003. Yield design of thin periodic plates by a homogenization technique and an application to masonry wall. C. R. Mécanique 331, 641–646.

Sanchez-Palencia, E., 1974. Comportement local et macroscopique d'un type de milieux physiques hétérogènes. Int. J. Eng. Sci. 12, 331–351.

Seremet, V.D., 1991. Handbook of Green's Functions and Matrices. Wit Press, Southampton.

Soize, C., 1993. Méthodes Mathématiques en Analyse du Signal. Masson, Paris.

Suquet, P., 1990. Une méthode simplifiée pour le calcul des propriétés élastiques de matériaux hétérogènes à structure périodique. C. R. Acad. Sci. 311, 769–774.

Willis, J.R., 1977. Bounds and self-consistent estimates for the overall properties of anisotropic composites. J. Mech. Phys. Solids. 25, 185–202.

Willis, J.R., 1980. A polarization approach to the scattering of elastic waves. I. Scattering by a single inclusion. J. Mech. Phys. Solids 28, 287–305.

Willis, J.R., 1981. Variational and related methods for the overall properties of composites. Advanced in Applied Mechanics. 21, 1–78.